CAPACITIVE EFFECTS ON QUANTITATIVE DOPANT PROFILING WITH SCANNED ELECTROSTATIC FORCE MICROSCOPES

Todd Hochwitz, Albert K. Henning, Chris Levey, and Charles Daghlian
Dartmouth College
Hanover, NH 03755
and
James Slinkman
IBM Microelectronics
Essex Junction, VT 05452

A force-based scanning Kelvin probe microscope has been applied to the problem of dopant profiling in silicon. Initial data analysis assumed the detected electrostatic force couples the sample and only the tip at the end of a force sensing cantilever. Attempts to compare measurements quantitatively against device structures with this simple model failed. We have determined a significant contribution arises from the electrostatic force between the sample and the entire cantilever, which depends strongly upon the relative size of the tip, cantilever, and lateral inhomogeneities in the surface topography and material composition of the sample. We present actual and simulated measurements which demonstrate the characteristic signature of this effect.

INTRODUCTION

Qualitative measurements taken with a combination of atomic force microscope (AFM) and scanning Kelvin probe microscope (SKPM) on simple implanted structures in silicon have been reported by several researchers (1–6). We report in (6) that initial attempts to quantify the measurements against theoretical models have not been completely successful. Further work on the samples described in (6) is reported here.

One of the most significant reasons for the reported discrepancy between measured surface potential profiles obtained via the SKPM and profiles predicted by theoretical models is the interaction between the cantilever of the force sensing probe, in addition to the tip, and the sample surface. We present and extend the usual electrostatic force model to show this discrepancy and present both simulation and experimental results which illustrate this interaction.

MODELS

We distringuish between a cantilever, a tip, and a probe. For this work the cantilever is the section of the force sensor which undergoes mechanical deflection. The tip is assumed to be physically attached to the cantilever. It is the location of primary force interaction with a sample under investigation. The probe consists of both the cantilever and the tip.

The mechanical deflection of a cantilever due to an electrostatic force between the probe and sample has been examined by several researchers and treated as a capacitive system (1, 7–9). The force on the probe due to a potential difference between the probe and sample may be represented as (2):

$$F_e = -\frac{1}{2}V^2C' \tag{1}$$

$$C' = \left(\frac{C_{\text{eff}}}{C_{\text{air}}}\right)^2 \frac{\partial C_{\text{air}}}{\partial z} \tag{2}$$

where V is the total potential difference, z is the spatial distance, C_{air} is the effective capacitance and $\frac{\partial C_{\text{air}}}{\partial z}$ is the spatial derivative of the effective capacitance between the probe and sample, and C_{eff} is the total capacitance in series with the system (including C_{air}).

The above equations are most applicable to a system where the sample and probe are metals. In this case the only spacing-dependent capacitance between the probe and the sample is across the air gap. If either the probe or the sample is a non-degenerately doped semiconductor, however, the total charge contained within a volume near the surface may also vary as the probe/sample spacing changes. This results in a different form of Equation 2. In addition, filled surface states may lead to a different electrostatic force than predicted by Equation 1.

Theoretical analysis indicates the cantilever deflection is directly proportional to the magnitude of this force (10). Thus, variations in the electrical nature of the probe/sample system can be examined by detecting and properly adjusting for changes in the mechanical deflection of the cantilever.

With the scanning electrostatic force microscope (SEFM) the potential difference V between the probe and sample can be comprised of a dc signal and/or one or more ac signals. With the SKPM the potential difference V consists of one dc component and one ac component, which may be represented as follows:

$$V = V(t) = V_{DC} - \frac{\Delta\Phi}{q} + V_{ac}\sin(\omega t) \tag{3}$$

where V_{DC} is the magnitude of the dc component applied by any external electronics, $\Delta\Phi$ is the work function difference (WFD) (in eV) of the materials, V_{ac} is the peak magnitude of the ac component of the externally applied potential between the probe and the sample, and ω is the frequency at which the ac voltage is oscillating.

If V in Equation 1 is replaced by the form given in Equation 3 and expanded, one obtains:

$$F_e = \frac{1}{2}\left(\left(V_{DC} - \frac{\Delta\Phi}{q}\right)^2 + \frac{1}{2}V_{ac}^2\right)C' \tag{4}$$

$$+ \quad C'\left(V_{DC} - \frac{\Delta\Phi}{q}\right)V_{ac}\sin(\omega t) \tag{5}$$

$$+ \quad \frac{1}{4}C'V_{ac}^2\cos(2\omega t) \tag{6}$$

The negative sign from Equation 1 has been removed since the mechanical deflection of the cantilever is proportional to the magnitude of the force. An interferometer is used to monitor cantilever deflections at the frequencies of ω and 2ω. The deflection at 2ω, which is proportional to Equation 6, yields sample capacitance information. The signal detected at ω, which is proportional to Equation 5, is used to minimize the electrostatic force. Since the capacitive and ac terms of Equation 5 are non-zero, the primary method to minimize cantilever deflection at ω is to adjust V_{DC} until it equals the WFD between sample and probe.

Ideally, the spatial variations in this feedback signal are used to estimate changes in the sample's surface work function (WF). In practice the feedback signal is equal to the WFD only for samples with surface features significantly larger than the entire probe. Our experience shows it is necessary to consider the interaction of all the electrically conductive components of the force sensing probe and sample surface, as suggested by other researchers (8, 11, 12).

Since the sample surface varies under the probe, the value of V_{DC} which minimizes the cantilever deflection becomes a weighted average of the WFD and capacitive components between the probe and the sample surface. This is analogous to the stray capacitance problems associated with the vibrating reed Kelvin probes (13–17). The impact of the errors is very different in the two techniques, so a direct application of prior analysis is not appropriate.

An example of this stray capacitance for the force-based SKPM is shown in Figure 1. It shows the profile of a micro-fabricated silicon force sensing probe (18) used in our system as it scans at a height of Z_O over a rectangular surface feature with vertical dimension ΔS. In general the total capacitance between the probe and sample would be an integral computed over the entire electrically active surface (12). For this work the capacitive components will be treated discretely to simplify the discussion and numerical analysis.

The total load shown in Figure 1 between the electrical connections to the sample and probe is modelled as three parallel capacitances. One component is between the end of the cantilever and the sample, the second component is between the tip and the feature of interest, and the third is between the bulk of the cantilever and the sample. Since these

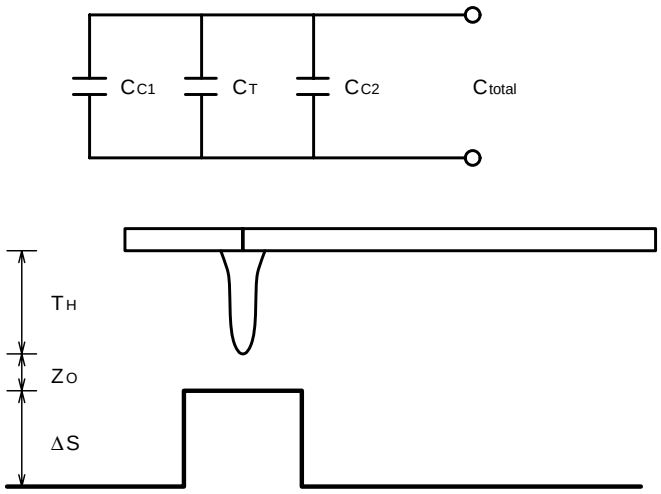

Figure 1: Schematic representation of the probe/sample subsystem and the equivalent capacitance circuit. The desirable capacitance is between the tip and the sample surface (C_T). The remaining cantilever and sample overlap yields stray capacitance (C_{C1} and C_{C2}). The tip is kept within tens of nanometers from the sample surface (Z_O) while the cantilever is several microns above the tip (T_H).

components are in parallel, the total effective capacitance is a sum of the individual capacitors. These capacitances are also in series to any additional capacitance between the electrical connections and the air gap, which for now are assumed to be constant for each branch.

The entire system can be broken down further and modelled as several very small capacitors in parallel, with the effective capacitance given as:

$$C_{total} = \sum_i C_i \tag{7}$$

where C_i is the contribution from each capacitive term. The derivative of C_{total} taken with respect to the vertical displacement between the sample and probe becomes:

$$\frac{\partial C_{total}}{\partial z} = \sum_i \frac{\partial C_i}{\partial z} \tag{8}$$

This changes the nature of Equation 5. The electrical signal S_ω obtained from a lock-in amplifier becomes:

$$S_\omega \propto V_{ac} \sum_i \frac{\partial C_i}{\partial z} \left(V_{DC} - \frac{\mathbf{\Delta\Phi}_i}{q} \right) \tag{9}$$

The applied voltage V_{DC} needed to minimize the deflection of the cantilever at ω is derived as follows:

$$\sum_i \frac{\partial C_i}{\partial z} \left(V_{DC} - \frac{\mathbf{\Delta\Phi}_i}{q} \right) = 0 \tag{10}$$

$$V_{DC} \sum_i \frac{\partial C_i}{\partial z} - \sum_i \frac{\partial C_i}{\partial z} \frac{\mathbf{\Delta\Phi}_i}{q} = 0 \tag{11}$$

$$V_{DC} \sum_i \frac{\partial C_i}{\partial z} = \sum_i \frac{\partial C_i}{\partial z} \frac{\mathbf{\Delta\Phi}_i}{q} \tag{12}$$

resulting in the final relationship

$$V_{DC} = \frac{\sum_i \frac{\partial C_i}{\partial z} \frac{\mathbf{\Delta\Phi}_i}{q}}{\sum_i \frac{\partial C_i}{\partial z}} \tag{13}$$

In addition, Equation 6 will also be modified. The capacitive term will be replaced with the summation from the denominator of Equation 13. Therefore, the capacitance signal will play an important role in extracting quantitative WFD results from the V_{DC} required to minimize the electrostatic force.

This is a simplified description of the contribution from the various capacitive components to the detected cantilever deflection. To model the cantilever deflection correctly, one would need to perform a self-consistent calculation of the equations of motion with the contributions from the entire probe. As described earlier, the summation is an approximation to the integral that would be required to obtain the exact relationship between the tip voltage and material parameters.

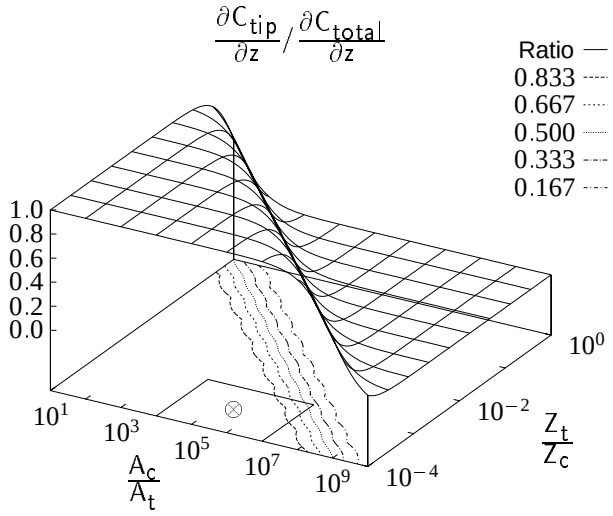

Figure 2: A surface plot showing the relative contribution of the tip/sample capacitance compared to the total probe/sample capacitance as functions of the area and sample spacing over a topographically flat surface ($\Delta S = 0$). A_c/A_t is the ratio of the cantilever area to the tip area and Z_t/Z_c is the ratio of the tip/sample spacing to the cantilever/sample spacing. Z_t corresponds to Z_O, and Z_c to $Z_O + T_H$, from Figure 1.

The simple analysis indicates the feedback voltage depends upon the lateral extents of the surface topography, dielectric properties, and WFD over the electrically active area between the probe and the sample. In order to obtain high resolution, it is necessary for most of the contribution to come from the interaction of the tip/sample and not the cantilever/sample. Figure 2 shows a plot of the following relationship:

$$\frac{\frac{\partial C_{tip}}{\partial z}}{\frac{\partial C_{tip}}{\partial z} + \frac{\partial C_{cantilever}}{\partial z}} \tag{14}$$

where $\frac{\partial C_{tip}}{\partial z}$ is the effective tip/sample capacitance and $\frac{\partial C_{cantilever}}{\partial z}$ is the effective cantilever/sample capacitance. This relationship is plotted as a function of the normalized areas and separation, assuming a topographically flat perfect conductor. The capacitance was treated as a parallel plate, so the curve shown is applicable only to systems that may be described as being proportional to an effective surface area and inversely proportional to the electrode spacing. The shape of the curve for other systems will vary, but the trends should remain similar.

The silicon probes we have been using are fabricated to be $\approx$ 100 μm long $\times$ 20 μm wide. The tip has a radius of curvature of $\approx$ 20 nm when sharp, and $\approx$ 0.3 to 0.5 μm when dulled after many scans or due to tip crashes. The normalized area of cantilever to tip lies in the range of 10^3 to 10^6. The van der Waals (vdW) control loop of our system is typically set to keep the tip $\approx$ 5 nm from the surface (Z_O in Figure 1), and the tip length is specified to be in the range of 6.5 to 7.0 μm (T_H in Figure 1). The normalized tip/sample to cantilever/sample spacing is less than 10^{-3}. This puts our operating area within the marked section of the plot ($\otimes$).

More than 99% of the capacitance comes from the tip/sample for dull tips. For sharp tips this drops to only 63%. If

we attempt to increase our resolution by fabricating finer tips, or if there is significant relief in the surface topography changing the spacing ratio, the tip capacitance ratio drops below 50%. Even if the feature under investigation is only as large as the effective area of the tip, the feedback voltage will not be the same as the material WFD unless the cantilever is also above material with a similar WF.

This is qualitatively consistent with the behavior of our system. We obtain much better contrast with dull tips, but at a loss in lateral resolution. Measurements taken with tungsten probes yield more constrast due to the larger effective tip area and a value of T_H in excess of 150 μm.

SIMULATION RESULTS

In order to determine the impact of this modified formulation upon the expected measurements, we computed Equation 13 for various types of probes and samples. The probe was divided into several elements, as shown in Figure 3. For each of these elements, the corresponding C_i, $\frac{\partial C_i}{\partial z}$, and $\frac{\Delta\Phi_i}{q}$ were computed between the i-th element of the probe and the nearest point on the model of the sample's surface. The capacitance between the i-th element and the surface was treated as a parallel plate in order to speed computation.

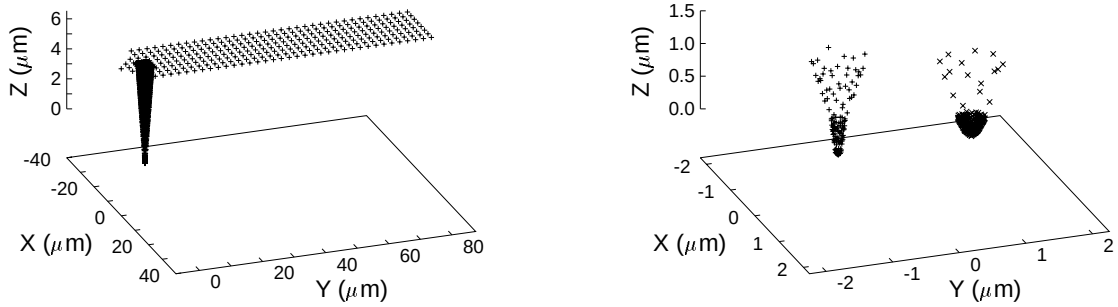

Figure 3: Plots showing the elements used to model the cantilever, a sharp ($+$) tip, and a dull ($\times$) tip of a force sensing probe. The cantilever is 20 μm wide $\times$ 100 μm long. The sharp tip has a radius of curvature of $\approx$ 20 nm, and the dull tip has a radius of curvature of ≈ 0.25 μm.

A finite element model (FEM) was used to represent the surface characterisitics of the sample. The values of the surface height, material WF, and effective substrate capacitance are stored for each point in the FEM mesh. The resulting tip voltage of Equation 13 is computed for each point in the mesh. For every probe element that does not lie on a mesh node, or when a computed value is desired for the surface at a point that does not lie on a mesh node, the values are computed via linear interpolation.

Figure 4 shows a perspective plot of the topography associated with the doped structures described in (6). There is an anomalous structure in the figure from the plotting package – it is not present in the actual mesh data. Figure 5 shows profiles of the effective substrate capacitance and WF for a slice taken through the middle of the structures. The values were representative of SIMS profiles and theoretical models for this particular sample.

A simulation of the scan was then performed with four types of probes. Two of the probes had sharp tips, and two had dull tips. For each pair, one probe was all silicon and the other had a silicon tip and gold cantilever. We did not simulate an all gold probe because our experience indicates that the gold tends to flake off, or the tip dulls, after extended use.

Figure 6 shows the simulated surface potential profiles for each of these four probes. The profiles are taken perpendicular to the direction of the simulated scan. The bulk of the cantilever was directed to the left. During the simulated scan the tip of the probe reaches the structures before the body of the cantilever, which mirrors the experimental procedure.

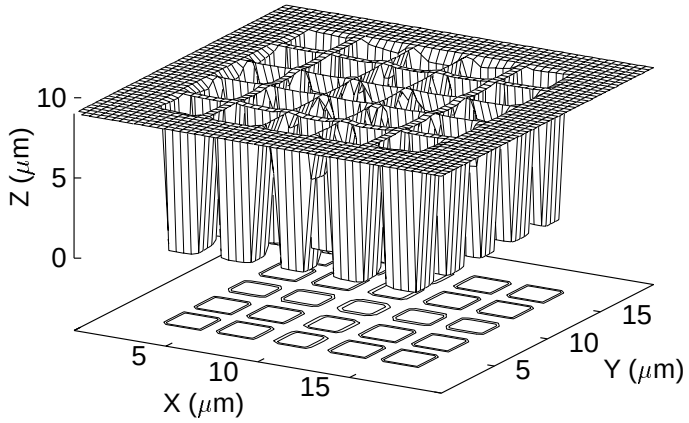

Figure 4: Plot of the idealized surface topography for the model of the dopant contacts described in (6). The contact holes are arranged in 5×5 arrays, with a width of 2 μm for each contact hole. The depth of each contact is 9 nm.

As predicted by our model, and consistent with behavior of our SKPM, more contrast is indeed predicted with a dull tip compared to a sharp tip. There is slope in the predicted signal, which is related to how much of the cantilever resides over the structures. The contrast is larger for the right structure because the cantilever is interacting with all five implant regions. There are also effects seen in the profile due to the physical edges of the surface.

One interesting item is the change in contrast for a sharp Si/Au probe, where the predicted surface potential for the implanted structures is actually less than that predicted by theory (compare to Figure 5). In several experimental

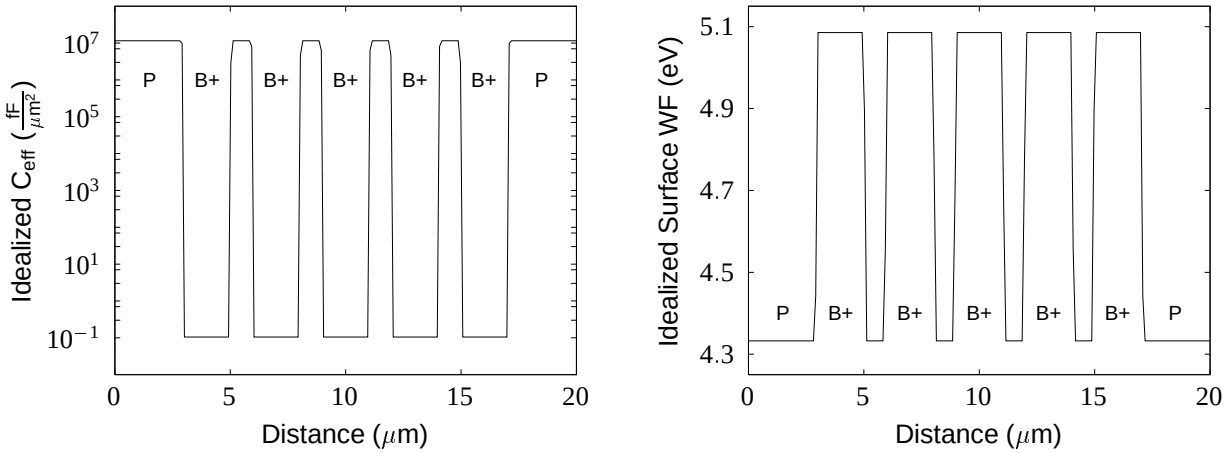

Figure 5: Profiles of the idealized effective surface capacitance and work function used in the model. The substrate is assumed to have 5 nm of oxide present. The capacitance within the contact holes is a much lower value due to the junction capacitance of the implanted *p*/*n* depletion region being in series with the surface oxide. The substrate was *n*-type silicon, doped with phosphorus to a density of 10^{14} cm^{-3}, with a work function of 4.33 eV. The contact holes were doped with boron to a density of 10^{19} cm^{-3}, with a work function of 5.09 eV.

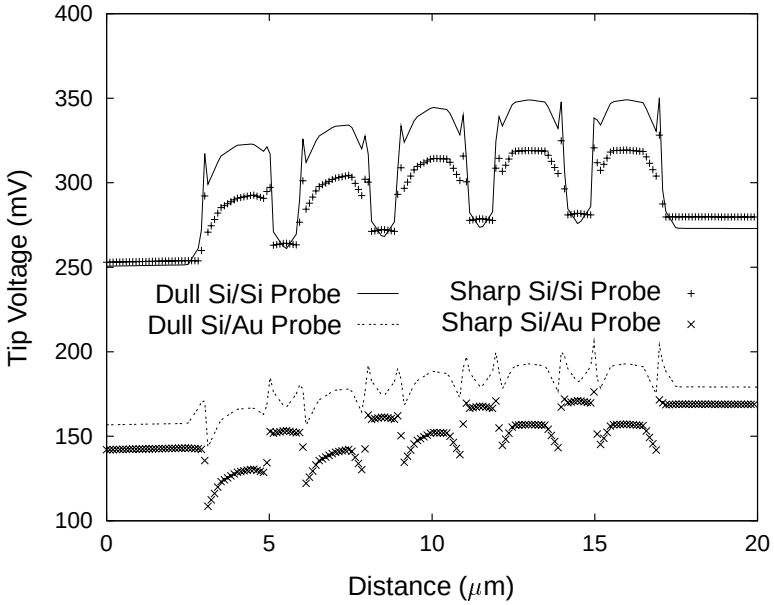

Figure 6: Profiles of the simulated tip voltage. The profiles are taken through the five contact holes in the middle of the array, and perpendicular to the direction of the simulated scan. The first scan line lies to the left of the array, and the final scan line lies to the right of the array. The results depend strongly upon how much of the tip and cantilever lie above the array, in addition to the material properties of the tip and cantilever.

situations a contrast change was found in the SKPM measurements. This change depends upon the settings of the van der Waals control loop when using coated probes. We attribute this to changes in the relative contributions of the Si/sample and Au/sample WFDs to the deflection of the cantilever.

Future software revisions will include self-consistent solutions to the van der Waals and electrostatic forces. This change will allow circumvention of the approximations present in Equation 13.

EXPERIMENTAL RESULTS

We present here measurements made with the SKPM on the samples described in (6). The measurements were performed upon structures in a different area of the test die, and so are not identical to previously published results. The test die contains several test structures grouped together in different sizes.

The measurements reported in (6) were taken near a center group. These measurements are taken near an edge group. As shown in the previous section, when the cantilever covers a larger number of the implanted structures the signal better approximates the true WFD. The previously published measurements show a wider signal swing than the ones in this manuscript, consistent with the model presented earlier.

Figure 7 shows the actual measurement profiles obtained with the SKPM. To remain consistent with the simulation results, the lines are taken perpendicular to the direction of the scan. The leftmost signal peaks correspond to implants that are in the interior of an array, and the rightmost peaks are on the edge of the implanted array.

The absolute value of the tip voltage does not match the simulated value. This difference is likely due to the condition of either the sample or probe surface. The signal swing of the simulation was ≈ 75 mV, whereas for the measured data it was ≈ 110 mV. Possible reasons for this discrepancy are uncertainty in the dopant concentrations near the surface of either the sample or probe, incorrect p/n junction capacitance or oxide thickness, incorrect probe/sample spacing, incorrect tip size, coarse discretization of the sample mesh used in the simulations, an invalid assumption that only the

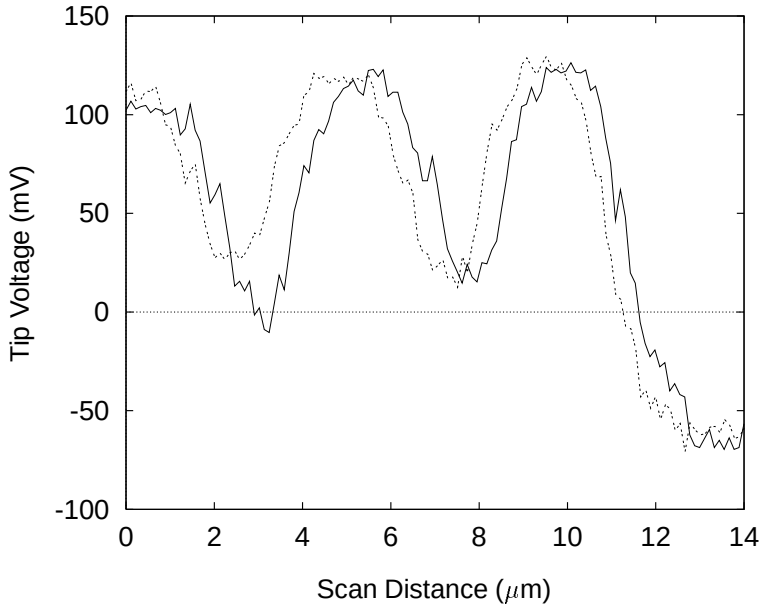

Figure 7: Profiles of the actual tip voltage from measurements performed on a fabricated structure of contact holes. The profiles are taken perpendicular to the scan direction in order to match the conditions of the profile shown in Figure 6. The peaks exhibit a slope similar to that shown in Figure 6, and the edges show a similar discontinuity. The discontinuity in the simulation is stronger due to the approximations used in the model.

capacitance across the air gap depends upon the tip/sample spacing, ignoring the presence of surface states or a thin water layer, ignoring the interaction of the laser with the silicon probe, off-axis orientation of the probe and sample surface, and/or interaction with structures on the sample surface that were not included in the FEM mesh.

Though the results are not quantitatively exact, they are qualitatively similar. The measured data show a similar slope in the signal as more of the cantilever covers the implant areas. There are discontinuities seen along the edges of the implant areas (they are not as strong as in the simulation results due to the method of numerical analysis), and the crowns of the features are rounded.

CONCLUSION

A simple extension of the electrostatic force model leads to theoretical results closer to the actual surface potential profiles measured with a force-based SKPM than is obtained with a traditional model. We have concentrated our discussion here upon the analysis of previously published measurements (6). The analysis has also been applied to other simple doped structures, including step- and stripe-like features. These results will be presented elsewhere.

The role of the cantilever cannot be ignored in the quantitative analysis of data obtained with an SEFM, especially where claims about the lateral resolution are made. The greatest impact will occur in dc measurements (the Kelvin mode), since the WF is essentially a dc signal with an infinite lateral extent. There will be less impact on the ac measurements (19–21) if the separation of signal lines carrying the ac signals is much larger than the cantilever size. When the cantilever lies over two different lines carrying signals at the same ac frequency, or when it lies over a significant portion of a single line, the probe signal will not reflect the actual tip/surface signal (amplitude and phase). The presence of the extra capacitance will also have an impact upon the amount of current drawn through the system, which may influence the sample under study.

To make more quantitative statements about the measurements will require deconvolution of the data. Our future research includes the formulation of a robust technique to extract the actual WFD and capacitance variations from the

electrostatic and capacitance measurements obtained with the SKPM.

ACKNOWLEDGMENTS

The authors acknowledge the following sources with gratitude: P. Cadrecha and the management of IBM – Essex Junction for equipment and personnel support; research support (for TH and AKH) through an IBM Shared University Research Grant, an Analog Devices Career Development Professorship, and Thayer School of Engineering funds; and M. O'Boyle for discussions related to the Kelvin measurements. This manuscript was prepared using LaTeX (22) and dvips (23). Figures were generated with xfig (24), gnuplot (25), and psfrag (26).

REFERENCES

1. Y. Martin, D. W. Abraham, and H. K. Wickramasinghe, Appl. Phys. Lett. **52**, 1103 (1988).
2. D. W. Abraham, C. C. Williams, J. Slinkman, and H. K. Wickramasinghe, J. Vac. Sci. Technol. B **9**, 703 (1991).
3. J. M. R. Weaver and D. W. Abraham, J. Vac. Sci. Technol. B **9**, 1559 (1991).
4. J. M. R. Weaver and H. K. Wickramasinghe, J. Vac. Sci. Technol. B **9**, 1562 (1991).
5. M. Nonnenmacher, M. O'Boyle, and H. K. Wickramasinghe, Ultramicroscopy **42–44**, 268 (1992).
6. A. K. Henning, T. Hochwitz, J. Slinkman, J. Never, S. Hoffmann, P. Kaszuba, and C. Daghlian, J. Appl. Phys. **77** (1995).
7. G. M. McClelland, R. Erlandsson, and S. Chiang, in *Review of Progress in Quantitative Nondestructive Evaluation*, edited by D. O. Thompson and D. E. Chimenti (Plenum, New York, 1987), Vol. 6B, p. 1307.
8. H. W. Hao, A. M. Baró, and J. J. Sáenz, J. Vac. Sci. Technol. B **9**, 1323 (1991).
9. D. Sarid, *Scanning Force Microscopy with Applications to Electric, Magnetic, and Atomic Forces, Oxford series in optical and imaging sciences* (Oxford University Press, New York, 1991).
10. D. Sarid and V. Elings, J. Vac. Sci. Technol. B **9**, 431 (1991).
11. G. E. Bridges and D. J. Thomson, Ultramicrosc. **42–44**, 321 (1992).
12. H. Yokoyama and T. Inoue, Thin Solid Films **242**, 33 (1994).
13. W. Thompson (Lord Kelvin), Phil. Mag. **46**, 82 (1898).
14. W. A. Zisman, Rev. Sci. Instrum. **3**, 367 (1932).
15. P. P. Craig and V. Radeka, Rev. Sci. Instrum. **41**, 258 (1970).
16. J. Bonnet, L. Soonckindt, and L. Lassabatère, Vacuum **34**, 693 (1984).
17. F. Rossi, Rev. Sci. Instrum. **63**, 4174 (1992).
18. O. Wolter, T. Bayer, and J. Greschner, J. Vac. Sci. Technol. B **9**, 1353 (1991).
19. A. S. Hou, F. Ho, and D. M. Bloom, Elect. Lett. **28**, 2302 (1992).
20. C. Böhm, C. Roths, U. Müller, A. Beyer, and E. Kubalek, Mat. Sci. Eng. **B24**, 218 (1994).
21. R. A. Said, G. E. Bridges, and D. J. Thomson, Appl. Phys. Lett. **64**, 1442 (1994).
22. TeX by D. Knuth and LaTeX by L. Lamport. Available via anonymous ftp from one of the Comprehensive TeX Archive Network (CTAN) sites: ftp.dante.de (Internet address 129.206.100.192), ftp.tex.ac.uk (Internet address 134.151.44.19), and pip.shsu.edu (Internet address 192.92.115.10).
23. T. Rokicki, Radical Eye Software. Available via anonymous ftp from labrea.stanford.edu (Internet address 36.8.0.112) or one of the CTAN sites.
24. Originally written by K. Yap, current version maintained by B. Smith, with contributions from many authors. TransFig is written by M. Bicah, with contributions from many authors. Available via anonymous ftp from ftp.cs.cornell.edu (Internet address 128.84.218.75).
25. T. Williams and C. Kelley, with contributions from many authors. Available via anonymous ftp from ftp.dartmouth.edu (Internet address 129.170.16.4).
26. C. Barratt, available via anonymous ftp from isl.stanford.edu (Internet address 36.60.0.10).